Theoretical Study on the Electronic and Molecular Structures of $(C_5H_5)M(L)$ (M = Rh, Ir; L = CO, PH_3) and $M(CO)_4$ (M = Ru, Os) and Their Ability To Activate the C-H Bond in Methane

Tom Ziegler,*,† Vincenzo Tschinke,† Liangyou Fan,† and Axel D. Becke‡

Contribution from the Departments of Chemistry, University of Calgary, Calgary, Alberta, Canada T2N 1N4, and Queens University, Kingston, Ontario, Canada K7L 3N6.
Received January 23, 1989

Abstract: Nonlocal density functional calculations have been carried out on the electronic and molecular structures of $(C_5H_5)M(L)$ (L = CO, PH_3; M = Rh, Ir) (**a**) and $M(CO)_4$ (M = Ru, Os) (**b**). All systems are found to have a singlet ground state. Optimized geometries are reported for each system on the singlet ground state as well as the first excited triplet state. The coordinatively unsaturated 16-electron species X_nM = **a**,**b** are usually generated from the 18-electron systems X_nMY by photolytic (or in some cases thermal) dissociation of Y. Calculated dissociation energies are presented for Y = CO, PH_3, and H_2 in the case of X_nM = a and for Y = CO and H_2 in the case of X_nM = **b**. Complete reaction profiles have been calculated for the oxidative addition of H_2 and CH_4 to **a** and **b**. The addition reactions are found to be more facile for **a** than for **b**. It is argued that **a** is unique as a C-H activating agent in having only empty σ-type d-based orbitals interacting with the incoming C-H bond. Most other mononuclear d^8 systems, such as **b**, have empty as well as occupied σ-type metal-based orbitals, and the latter will impede the addition reaction. It is further argued that the high energy of the HOMO on **a** aids in the addition of H-H and H-CH_3 bonds to Cp(L)M. Calculations are presented on the reaction enthalpies of the H-H and C-H addition processes along with the M-H and M-CH_3 bond energies. The 5d elements are found to form stronger bonds than their 4d congeners as a result of relativistic effects as well as better bonding overlaps. Geometry optimizations were carried out on the dihydride and hydrido-alkyl complexes. Approximate transition-state structures are presented for the C-H addition reactions.

I. Introduction

Methane is an abundant commodity, which is difficult to functionalize into more valuable chemicals, primarily due to the strength of the C-H bond. Such a functionalization could be visualized[1] as taking place in the cycle of Scheme I, where CH_4 is functionalized by the feedstock Y to H-Y-CH_3 with L_nM as a catalyst. The addition of inexpensive feedstocks such as alkenes or alkynes would in Scheme I result in longer chained alkanes or alkenes, respectively, whereas CO would produce acetaldehyde.

A realization of the cycle in Scheme I was brought a good deal closer when Janowicz and Bergman[2] as well as Hoyano and Graham[3] demonstrated that $(C_5Me_5)IrL$ (L = CO, PMe_3) can add alkanes oxidatively according to the equation

$$(C_5Me_5)IrL + HR \rightarrow (C_5Me_5)(L)Ir(H)(R) \qquad (1)$$

The reaction in eq 1 constitutes an example of step b in Scheme I. The homologous rhodium system $(C_5Me_5)Rh(PMe_3)$ has also been shown[4a] to activate alkylic C-H bonds.

Generation of the coordinatively unsaturated catalyst $(C_5Me_5)IrL$, step a of Scheme I, has been accomplished by photolytic expulsion of CO[3]

$$(C_5Me_5)Ir(CO)_2 \xrightarrow{h\nu} (C_5Me_5)Ir(CO) + CO \qquad (2)$$

or[2] H_2

$$(C_5Me_5)(PMe_3)Ir(H)_2 \xrightarrow{h\nu} (C_5Me_5)(PMe_3)Ir + H_2 \qquad (3)$$

The d^8 systems, $(C_5Me_5)(L)M$ (M = Ir, Rh), are unique in that they are among the few late-transition-metal complexes capable of activating an alkylic C-H bond. Saillard and Hoffmann[5] have pointed out that the inability of most d^8 ML_4 systems to activate C-H bonds is related to their square-planar structure. They have suggested that d^8 ML_4 systems with an angular "butterfly" structure might be able to add an alkylic C-H bond oxidatively. The addition of an alkylic C-H bond to the d^{10} systems, $(PH_3)_2M$ (M = Pd, Pt), has been studied theoretically by Low[6] and Goddard. They find the addition reaction to be thermodynamically unfavorable with a large activation energy. Activation of C-H and C-C bonds have recently been reviewed by Crabtree.[4b] Crabtree[4c] et al. have also attempted to deduce the transition-state structure for the addition of a C-H bond to a metal center from experimental structures of agostic metal-alkyl complexes. The activation of H-H and C-H bonds on metal surfaces has been discussed by Upton.[4d]

Scheme I

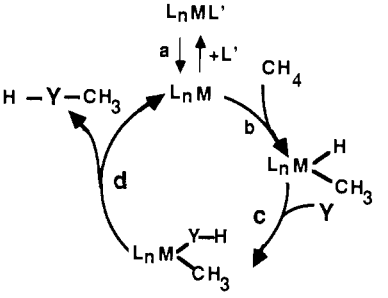

The objective of the present study is 3-fold. The first objective is related to step b in Scheme I. We would like to acquire a detailed understanding of the energetics and kinetics with regard to the addition of a C-H bond to a metal center. Calculations have to this end been carried out on the energy profile for the reaction in eq 1. We have in addition traced the profile for the reaction involving the rhodium system, CpRhL, in order to probe the different reactivity of the 4d and 5d congeners. We shall further attempt to gauge the unique features of the reaction in eq 1 by comparing its energy profile with the profile from the oxidative addition of CH_4 to $M(CO)_4$ (M = Ru, Os). The two

† University of Calgary.
‡ Queens University.

(1) Stoutland, P. O.; Bergman, R. G.; Nolan, S. P.; Hoff, C. D. *Polyhedron* **1988**, *7*, 1429.
(2) Janowicz, A. H.; Bergman, R. G. *J. Am. Chem. Soc.* **1982**, *104*, 352.
(3) Hoyano, J. K.; Graham, W. A. G. *J. Am. Chem. Soc.* **1982**, *104*, 3727.
(4) (a) Jones, W. D.; Feher, F. J. *J. Am. Chem. Soc.* **1982**, *104*, 4240. (b) Crabtree, R. H. *Chem. Rev.* **1985**, *85*, 245. (c) Crabtree, R. H.; Lavin, M. E.; Holt, E. M. *Inorg. Chem.* **1985**, *24*, 1986. (d) Upton, T. H. *J. Am. Chem. Soc.* **1984**, *106*, 1561.
(5) Saillard, J.-Y.; Hoffmann, R. *J. Am. Chem. Soc.* **1984**, *106*, 2006.
(6) Low, J. J.; Goddard, W. A. III *J. Am. Chem. Soc.* **1986**, *108*, 6115.

0002-7863/89/1511-9177$01.50/0

d^8 fragments $Ru(CO)_4$ and $Os(CO)_4$ are likely to have an angular butterfly structure. They might thus be able to add alkylic C–H bonds according to the analysis given by Saillard and Hoffmann.[5]

The second objective is related to step a of Scheme I and concerns the generation of the catalytically active and coordinatively unsaturated species ML_n. For the cycle in Scheme I to be efficient the dissociation energy in step a must be modest. We shall discuss the energy requirement for the generation of the Cp(L)M and $M(CO)_4$ fragments by thermal dissociation from the coordinatively saturated parent molecules Cp(L)MX and $M(CO)_4Z$ with X = CO, PH_3, H_2 and Z = CO, H_2.

The last objective is concerned with the molecular and electronic structures of Cp(L)M and $M(CO)_4$. Much attention[7] has been given to $Fe(CO)_4$, which in fact has a triplet ground state. What is the geometry and electronic ground state of the homologue ruthenium and osmium systems? Do they have an angular butterfly structure suitable for C–H activation? Much thought has also been given to the possible electronic and molecular structures of the Cp(L)M systems as reviewed by Hofmann and Padmanabhan[8] in their extended Hückel study. Hofmann and Padmanabhan were able to provide a very interesting and elegant analysis of the frontier orbitals in Cp(L)M. However, the extended Hückel method cannot calculate energy differences between singlet and triplet states. It was as a consequence not possible to determine the electronic ground state.

The present work is an extension of previous density functional[9,10] calculations on the strength of M–CO,[11a] M–H,[12] M–CH_3,[12] M–L,[12b] and M–M[13] bonds as well as elementary reaction steps[14] in organometallic chemistry, including a complete analysis[15] of all steps in the catalytic hydroformylation cycle. The present method seems correct[11–13] to reproduce the experimentally observed trends in M–L bond energies as a function of L as well as M. Deviations of up to 40 kJ mol^{-1} between calculated and experimental M–L bond energies have been encountered.[11a,12] However, these deviations are in most cases within experimental uncertainties.

II. Computational Details

The calculations presented here were carried out with the LCAO–HFS program system developed by Baerends[16] et al. and recently vectorized by Ravenek.[17] All relativistic calculations were based on the method due to Snijders[18] et al. Extensive use has been made of the numerical integration scheme developed by Becke.[19] Bond energies were evaluated by the generalized transition-state method,[20] and geometry optimizations were carried out according to the algorithm developed by Versluis[21] and Ziegler. Total energies, E, were evaluated according to

$$E = E_{HFS} + E_c + E_X^{NL} \quad (4)$$

Here E_{HFS} is the total statistical energy expression for the Hartree–Fock–Slater (HFS) or Xα method[22] and E_c and E_X^{NL} additional correction terms. The first correction term, E_c, has been proposed by Stoll[23] et al. It represents correlation between electrons of different spins, which is lacking in the original HFS method. The second correction terms, E_X^{NL}, has been proposed by Becke[19] and represents a nonlocal correction to the local HFS exchange energy. The correction term E_c was based on Vosko's parametrization[24] from electron gas data. Complete analytical expressions for E_{HFS} and E_X^{NL} are given in ref 22 and 19, respectively. The expression for E_c, based on the work by Vosko,[24] is defined in ref 23.

The molecular orbitals were expanded as a linear combination of Slater-type orbitals (STO).[16] An uncontracted triple-ζ STO basis set[25] was employed for the transition metals. The basis set on the ligands was of double-ζ quality. For all ligand atoms other than those on the Cp ring the basis was augmented by a single STO d-orbital ($\zeta_{3d}^C = 2.5$, $\zeta_{3d}^O = 2.0$, $\zeta_{3d}^P = 1.3$), with the exception of H where a 2p polarization STO function of $\zeta_{2p}^H = 1.0$ was used. A set of auxilliary[26] s, p, d, f, and g STO functions, centered on all nuclei, was used in order to fit the molecular density and present Coulomb and exchange potentials accurately in each SCF cycle. The orbitals in the upper ns, np, nd, (n + 1)s, and (n + 1)p shells on the metals and the upper ns, np shells on the ligands were considered as valence whereas orbitals in shells of lower energies were considered as core and frozen according to the procedure by Baerends[16] et al. Standard geometries were adopted for C_5H_5 (Cp), CO, and PH_3. The exchange factor[22] α_{ex} in the expression for E_{HFS} was given a value of $^2/_3$ in accordance with Becke's theory.[19]

III. Molecular and Electronic Structures of CpML (L = CO, PH_3; M = Rh, Ir) and $M(CO)_4$ (M = Ru, Os)

The electronic structure of the coordinatively unsaturated 16-electron d^8 fragment CpML (**1**) has been studied by Hofmann

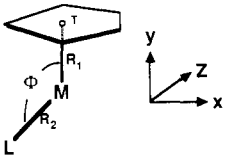

1

and Padmanabhan[8] for various ligands, L, and M = Co, Rh, and Ir. The CpML fragment of C_s point group symmetry (**1**) has at lower energy two occupied metal orbitals, 1a′ (**2a**) and 1a″ (**2b**) made up of $d_{x^2-y^2}$ and d_{xz}, respectively. Both d orbitals are stabilized by interactions with π^* orbitals on L. At somewhat higher energy is the occupied metal-based d_{z^2} orbital 2a′ (**2c**) with a weak M–L antibonding σ interaction. At highest energy are the two metal-based orbitals, 2a″ (**2d**) and 3a′ (**2e**), made up primarily of d_{yz} and d_{xy}, respectively. Both are destabilized by interactions

(7) Poliakoff, M.; Weitz, E. *Acc. Chem. Res.* **1987**, *20*, 408, and references therein.
(8) Hofmann, P.; Padmanabhan, M. *Organometallics* **1983**, *2*, 1273.
(9) Becke, A. *J. Chem. Phys.* **1986**, *84*, 4524. For a review of density functional theory, see ref 10.
(10) (a) Dahl, J. P., Avery, J., Eds. *Local Density Approximations in Quantum Chemistry and Solid State Physics*; Plenum Press: New York, 1984. (b) Erdahl, R. M., Smith, V. H., Jr., Eds. *Density Matrices and Density Functionals*; D. Reidel: Dordrecht, The Netherlands, 1987.
(11) (a) Ziegler, T.; Tschinke, V.; Ursenbach, C. *J. Am. Chem. Soc.* **1987**, *109*, 4825. (b) Huq, R.; Poe, A. J.; Chawla, S. *Inorg. Chim. Acta* **1979**, *38*, 121. (c) Lewis, K. E.; Golden, D. M.; Smith, G. P. *J. Am. Chem. Soc.* **1984**, *106*, 3906.
(12) (a) Ziegler, T.; Tschinke, V.; Becke, A. *J. Am. Chem. Soc.* **1987**, *109*, 1351. (b) Ziegler, T.; Tschinke, V.; Versluis, L.; Baerends, E. J.; Ravenek, W. *Polyhedron* **1988**, *7*, 1625. (c) Ziegler, T.; Wendan, C.; Baerends, E. J.; Ravenek, W. *Inorg. Chem.* **1988**, *27*, 3458. (d) Ziegler, T.; Snijders, J. G.; Baerends, E. J.; Ravenek, W. *J. Phys. Chem.*, in press.
(13) Ziegler, T.; Tschinke, V.; Becke, A. *Polyhedron* **1987**, *6*, 685.
(14) (a) Master, A. P.; Sorensen, T.; Ziegler, T. *Organometallics*, in press. (b) Ziegler, T.; Versluis, L.; Tschinke, V. *J. Am. Chem. Soc.* **1986**, *708*, 612.
(15) (a) Versluis, L.; Ziegler, T. *J. Am. Chem. Soc.*, in press. (b) Versluis, L.; Ziegler, T., submitted for publication in *J. Am. Chem. Soc.* (c) Versluis, L. Ph.D. Thesis, University of Calgary, Calgary, 1989.
(16) (a) Baerends, E. J.; Ellis, D. E.; Ros, P. *Chem. Phys.* **1973**, *2*, 71. (b) Baerends, E. J.; Ros, P. *Int. J. Quantum Chem.* **1978**, *S12*, 169. (c) Baerends, E. J.; Snijders, J. G.; de Lange, C. A.; Jonkers, G. In *Local Density Approximations in Quantum Chemistry and Solid State Physics*; Dahl, J. P., Avery, J., Eds.; Plenum: New York, 1984.
(17) Ravenek, W. In *Algorithms and Applications on Vector and Parallel Computers*; te Riele, H. J. J., Dekker, Th. J.; van de Vorst, H. A., Eds.; Elsevier: Amsterdam, The Netherlands, 1987.
(18) Snijders, J. G.; Baerends, E. J.; Ros, P. *Mol. Phys.* **1979**, *38*, 1909.
(19) Becke, A. D. *J. Chem. Phys.* **1988**, *88*, 2547.
(20) Ziegler, T.; Rauk, A. *Theor. Chim. Acta* **1977**, *46*, 1. The generalized transition-state method is not only applicable to the HFS scheme. It can be extended to any energy density functional such as the one by Becke in ref 9.
(21) Versluis, L.; Ziegler, T. *J. Chem. Phys.* **1988**, *88*, 322.
(22) Slater, J. C. *Adv. Quantum Chem.* **1972**, *6*, 1.
(23) Stoll, H.; Golka, E.; Preuss, H. *Theor. Chim. Acta* **1980**, *55*, 29.
(24) Vosko, S. H.; Wilk, L.; Nusair, M. *Can. J. Phys.* **1980**, *58*, 1200.
(25) (a) Snijders, G. J.; Baerends, E. J.; Vernooijs, P. *Atom. Nucl. Data Tables* **1982**, *26*, 483. (b) Vernooijs, P.; Snijders, G. J.; Baerends, E. J. Slater-type basis functions for the whole periodic system: Internal report; Free University: Amsterdam, The Netherlands, 1981.
(26) Krijn, J.; Baerends, E. J. Fit functions in the HFS method: Internal Report (in Dutch); Free University: Amsterdam, The Netherlands, 1984. Full information about the applied set of fit functions is available on request from the Calgary authors.

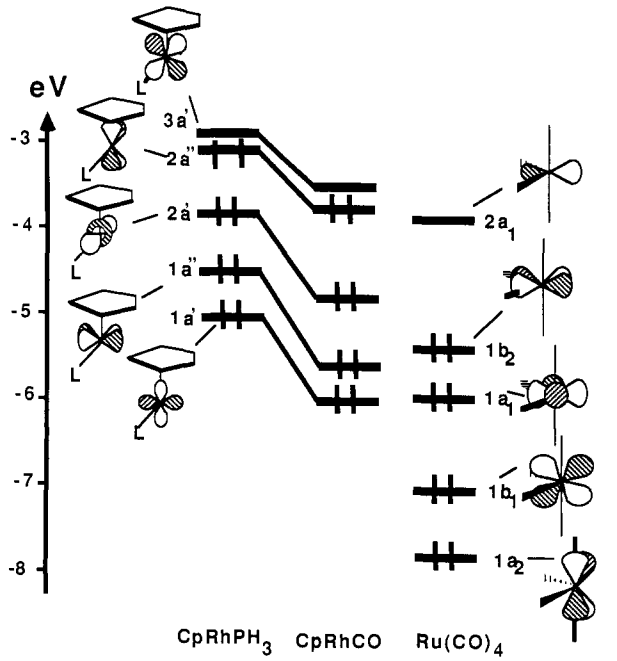

Figure 1. Orbital level diagrams for CpRhL (L = CO, PH_3) and $Ru(CO)_4$ in their singlet states. The orbital energies for the corresponding CpIrL and $Os(CO)_4$ systems are quite similar with the same ordering.

with occupied π orbitals on the Cp ring, and 3a′ of highest energy is in addition destabilized by the σ orbital on L.

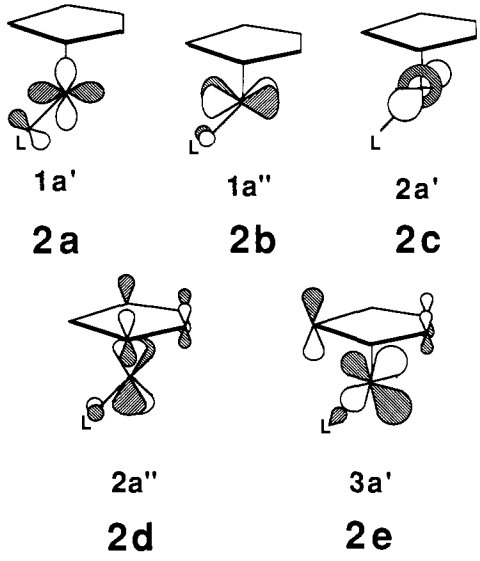

An orbital level diagram for the fragments CpRhL with L = CO and PH_3 is given in Figure 1. As expected, the relatively strong π acceptor, CO, is seen to stabilize the d levels more than the poorer π acceptor, PH_3. There are eight electrons to distribute among the d levels in Figure 1, and the close proximity between the 2a″ (**2d**) and 3a′ (**2e**) levels would thus suggest a relatively small energy splitting between the $^3A''$ triplet state with the electronic configuration $(1a')^2(1a'')^2(2a')^2(2a'')^1(3a')^1$ and the $^1A'$ singlet state with the electronic configuration $(1a')^2(1a'')^2(2a')^2(2a'')^2$.

We have optimized the key geometrical parameters of CpML (**1**) for both states and calculated the singlet–triplet splitting. We find the singlet state to be slightly more stable (5–25 kJ mol^{-1}) than the triplet state. The optimized structures for the rhodium systems are shown in Figure 2. The triplet systems exhibit a larger distance, R_1 (**1**), between the metal and the Cp ring center, T, as well as a larger Rh–L bond distance, R_2 (**1**), and the T–M–L bond angle, Φ.

The longer M–L bond in the triplet state reflects the fact that one electron is situated in the M–L σ antibonding orbital $3a_1$ (**2e**),

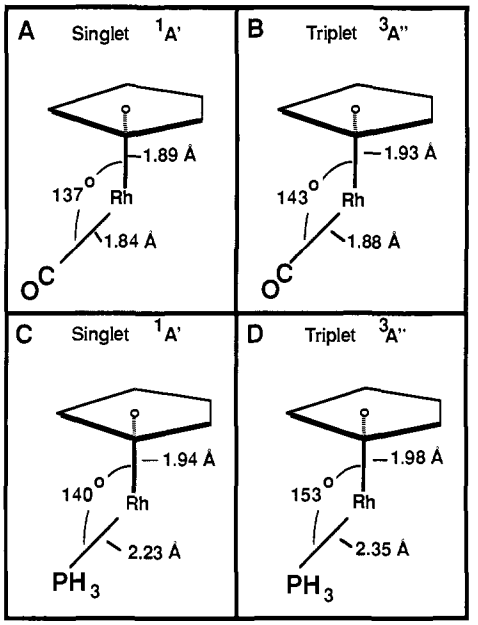

Figure 2. Molecular structures of CpRhL (L = CO, PH_3) for the $^3A''$ and $^1A'$ states. The structures for the corresponding CpIrL systems exhibit the same changes in going from the $^3A''$ state to the $^1A'$ state.

whereas this orbital is empty in the $^1A'$ singlet state. The M–L antibonding σ interaction in $3a_1$ (**2e**) can be reduced by increasing the Φ angle. The $^3A''$ triplet state has for this reason a larger Φ angle than the $^1A'$ singlet state (see Figure 2). The complete relief from the antibonding M–L interaction in 3a′ would require an opening of Φ to 180°. However, this limiting value is not realized, since 1a′ (**2a**) is destabilized by antibonding M–L σ interactions for $\Phi > 135°$. Note that the elongation of R_2 and the increase in Φ is most pronounced for the stronger σ donor PH_3.

The longer R_1 distance (**1**) in $^3A''$ compared to $^1A'$ (see Figure 2) reflects the fact that the antibonding interaction between the metal center and the Cp ring is somewhat stronger in 3a′ than in 2a″. The antibonding interaction between d_{yz} and the Cp ring orbital is reduced in 2a″ by mixing in the empty $(n + 1)p_z$ metal orbital (**3a**). A similar reduction could be obtained by mixing $(n + 1)p_x$ into 3a′ (**3b**). However, such an admixture would enhance the antibonding M–L σ interaction and does not take place to any significant extent. Instead, $(n + 1)p_y$ is mixed into d_{xy} of 3a′ in such a way as to reduce the antibonding M–L σ interaction. The admixture in **3c** does not have any net effect on the antibonding interaction with the Cp ring.

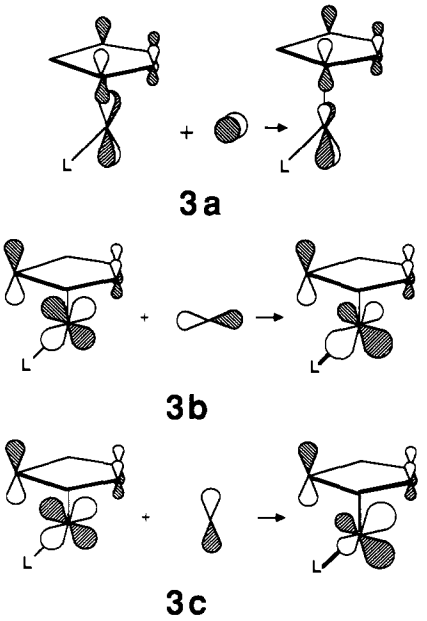

There have been some speculations as to whether the reactive d^8 intermediate CpML could decay to a lower lying $^3A''$ triplet state, after it is produced in the $^1A'$ singlet state by either of the processes in eq 2 or 3. The fact that the singlet state is calculated to be of lowest energy would indicate that CpML remains on the singlet surface after its formation. Consequently, the reactions in eq 1 will be considered as involving CpML in the $^1A'$ singlet state in the rest of this paper.

We shall also be interested in the 16-electron fragments $M(CO)_4$ (M = Ru, Os), in connection with our study of C–H activation. The frontier orbitals of the $M(CO)_4$ fragments, **4a** of C_{2v} symmetry are well-known.[27] Of lowest energy are the three

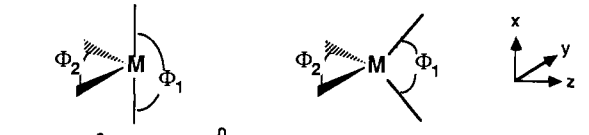

4a **4b**

metal-based orbitals $1a_2$ (**5a**), $1b_1$ (**5b**), and $1a_1$ (**5c**) primarily made up of d_{xy}, d_{xz}, and d_{z^2}, respectively.[28] At higher energy are the $1b_2$ (**5d**) orbital, derived from d_{yz}, and the (s,p,d) metal hybrid orbital $2a_1$ (**5e**).

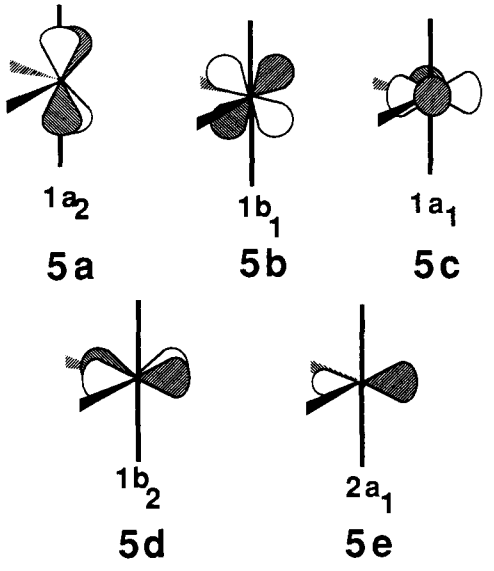

5a **5b** **5c** **5d** **5e**

The orbital energies of the $Ru(CO)_4$ and CpRhL fragments are compared in Figure 1. It is clear that the d orbitals in the $Ru(CO)_4$ fragment with four strongly π-accepting ligands are stabilized more than the d levels in CpRhL with, at most, one strongly π-accepting ligand. We have optimized the geometries for the $M(CO)_4$ fragment in the $^1A_1$ singlet state with the $(1a_2)^2(1b_1)^2(1a_1)^2(1b_2)^2$ configuration and the $^3B_2$ triplet state with the $(1a_2)^2(1b_1)^2(1a_1)^2(1b_2)^1(2a_1)^1$ configuration; see Figure 3. The $^1A_1$ singlet state was calculated to be more stable than the $^3B_2$ triplet state by 37 kJ mol^{-1} ($Ru(CO)_4$) and 42 kJ mol^{-1} ($Os(CO)_4$), respectively. The actual ground state has not been determined[29] for the $Ru(CO)_4$ and $Os(CO)_4$ systems. There have been some attempts[29a] to determine the electronic ground state for the homologous $Fe(CO)_4$ system. Thus a MCD study by Barton[29a] et al. has provided qualitative evidence for a $^3B_2$ ground state. However, it has not been possible to confirm this assignment by electron-spin resonance studies.[29b] Our calculations indicate that

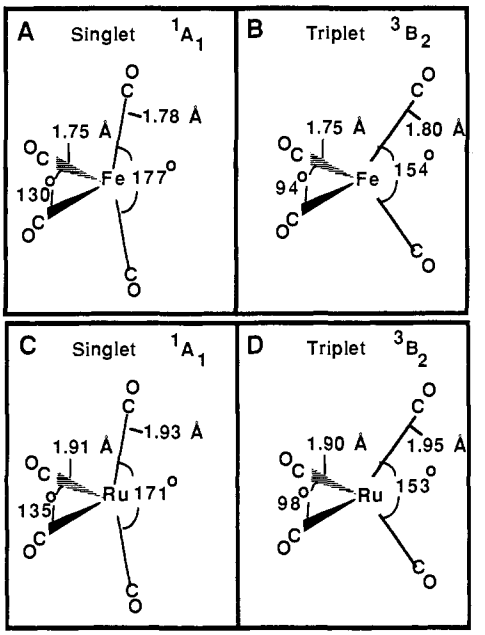

Figure 3. Molecular structures of $Fe(CO)_4$ and $Ru(CO)_4$ for the $^1A_1$ singlet states and $^3B_2$ triplet states. The $Os(CO)_4$ fragment exhibits the same trend in going from the $^1A_1$ singlet state to the $^3B_2$ triplet state.

the $^3B_2$ and $^1A_1$ states are very close in energy, with $^1A_1$ being of lowest energy by only 4 kJ mol^{-1}. It might well be that the $Fe(CO)_4$ system has a triplet ground state. Irrespective, it is not inconceivable that the ground state might change from high spin to low spin down the triad in a homologous series, given that the 3d member has stronger d–d exchange interactions than the 4d and 5d congeners.

The calculated $^1A_1$ and $^3B_2$ structures of $Fe(CO)_4$ and $Ru(CO)_4$, given in Figure 3, are intermediates between the butterfly conformation, **4a**, and the tetrahedral conformation, **4b**. The triplet structures (parts b and d of Figure 3) resemble the structure deduced for $Fe(CO)_4$ from IR spectroscopy by Poliakoff and Turner.[29c] They are best characterized as distorted tetrahedrons. The singlet geometries (parts a and c of Figure 3) resemble the distorted butterfly structure, **4b**. They could also be viewed as having a distorted square-planar conformation. The structures in Figure 3 are unique in that most d^8 ML_4 complexes are tetrahedral in the high-spin state and square-planar in the low-spin state. The driving force behind the distortions in Figure 3 for the d^8-carbonyl fragments $M(CO)_4$ has been analyzed elsewhere.[29d,30]

We have seen that the two d^8 systems $Ru(CO)_4$ and $Os(CO)_4$ in fact have an angular butterfly structure, **4a**, in their singlet ground state. The two systems are thus isolobal[5] with the Cp(L)M species since the HOMO's, **2d** and **5d**, as well as the LUMO's, **2e** and **5e**, are of the same nodal symmetry. Whether this analogy in fact will translate into a comparable ability to add H–H and C–H bonds oxidatively will be discussed in the next sections.

IV. Generation of CpML, $Ru(CO)_4$, and $Os(CO)_4$

The active 16-electron d^8 complexes of the type CpML can be generated by photolytic expulsion of CO from CpM(CO)L. This is an energetically demanding process as well as a kinetic bottleneck in any potential catalytic cycle involving C–H activation by CpM(CO)L (see Scheme I). An attractive alternative route would involve thermal dissociation of either a CO ligand

$$Cp(L)MCO \xrightarrow{\Delta} Cp(L)M + CO \qquad M = Rh, Ir;\ L = CO, PH_3 \quad (4a)$$

or a phosphine ligand

$$Cp(L)MPH_3 \xrightarrow{\Delta} Cp(L)M + PH_3 \qquad M = Rh, Ir;\ L = CO, PH_3 \quad (4b)$$

(27) (a) Elian, M.; Hoffmann, R. *Inorg. Chem.* **1975**, *14*, 1058. (b) Burdett, J. K. *Inorg. Chem.* **1975**, *14*, 375.

(28) The d component in the $1a_1$ orbital is 92% d_{z^2} in the singlet state. In the triplet state it is 75% d_{z^2} and 25% $d_{x^2-y^2}$.

(29) (a) Barton, T. J.; Grinter, R.; Thomson, A. J.; Davis, B.; Poliakoff, M. *J. Chem. Soc., Chem. Commun.* **1977**, 841. (b) Lionel, T.; Morton, J. R.; Preston, K. F. *J. Chem. Phys.* **1982**, *76*, 234. (c) Poliakoff, M.; Turner, J. J. *J. Chem. Soc., Dalton Trans.* **1974**, 2276. (d) Daniel, C.; Benard, M.; Dedieu, A.; Wiest, R.; Veillard, A. *J. Phys. Chem.* **1984**, *88*, 4805.

(30) Albright, T. A.; Burdett, J. K.; Wangbo, M. H. In *Orbital Interactions in Chemistry*; Wiley: New York, 1985.

Table I. Calculated $L_nM\ L'$ Ligand Dissociation Energies, $D(L_nM\ L')$

ML_n	L'	$D(L_nM\ L')$, kJ mol^{-1} M = Rh	M = Ir
Cp(CO)M	CO	191	239
$Cp(PH_3)M$	CO	183	233
Cp(CO)M	PH_3	121	134
$Cp(PH_3)M$	PH_3	132	138

Thermal ligand dissociation from a saturated 18-electron species is an integral part of the hydroformylation process[15] and other important catalytic cycles. We have calculated the experimentally unknown ligand dissociation energies corresponding to the processes in eq 4. We find, Table I, that the Rh–PH_3 and Ir–PH_3 bonds are moderately labile with M–PH_3 dissociation energies in the range of 125–150 kJ mol^{-1}. It should thus be possible to generate the active intermediate CpML from eq 4b. The Rh–CO and Ir–CO bonds are much more robust with M–CO dissociation energies ranging from 180–190 kJ mol^{-1} for M = Rh to 220–230 kJ mol^{-1} for M = Ir. It is for this reason not likely that CpML can be generated thermally according to eq 4a at modest temperatures. Our findings, Table I, are in line with kinetic measurements on ligand substitution reaction involving $CpM(L)_2$ (L = CO, PR_3). For L = CO ligand substitution takes place by an associative mechanism[31] without prior M–CO dissociation, whereas, the substitution reaction with L = PR_3 in some instances[32] is dissociative.

We have previously[11a] calculated the first CO dissociation energy for $Ru(CO)_5$ and $Os(CO)_5$ as 92 and 98 kJ mol^{-1}, respectively. One would thus expect that the two coordinatively unsaturated $M(CO)_4$ species are formed readily by thermal CO expulsion, and this is in fact what is observed experimentally. Experimentally[11b] the first CO dissociation energy for $Ru(CO)_5$ has been estimated as 117 kJ mol^{-1}. The corresponding experimental value for $Os(CO)_5$ is not available. It is interesting to note that the first CO dissociation energy for $Fe(CO)_5$ is much higher with an experimental value[11c] of 176 KJ mol^{-1} and a theoretical value[11a] of 176 kJ mol^{-1}. The decrease in the first CO dissociation energy down a triad has been rationalized in ref 11a.

Why is the M–CO linkage much weaker in $M(CO)_5$ than in Cp(L)MCO? In the first place, five strongly π-accepting CO ligands are competing for electron density on the metal center in $M(CO)_5$. This competition is less severe in Cp(L)MCO where the Cp ring acts as a modest π acceptor. Of even more importance is the fact that the σ_{CO} orbital in $M(CO)_5$ suffers (**6a**) a two-orbital four-electron repulsive interaction with the d_{z^2} orbital **5c** on the $M(CO)_4$ fragment, whereas σ_{CO} in Cp(L)MCO interacts (**6b**) with the empty d_{xy} orbital (**2e**) on Cp(L)M. The adverse role played by the orbitals **5c** and **2e** will be of crucial importance in our analysis of the interaction between either H_2 or CH_4 and the two metal fragments $M(CO)_4$ and Cp(L)M.

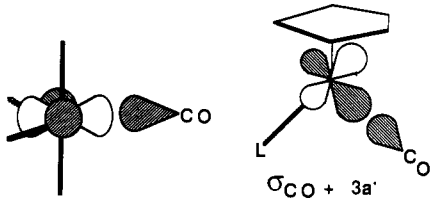

6a **6b**

The active CpML complex has also been generated[2] by photolytic expulsion of H_2 from the dihydride $Cp(L)M(H)_2$ according to the reaction

$$Cp(L)M(H)_2 \rightarrow CpML + H_2 \qquad M = Rh, Ir;\ L = CO, PR_3 \quad (5a)$$

(31) Basolo, F. *Coord. Chem. Rev.* **1982**, *43*, 7.
(32) Janowicz, A. H.; Brundza, H. E.; Bergman, R. G. *J. Am. Chem. Soc.* **1981**, *103*, 1516.

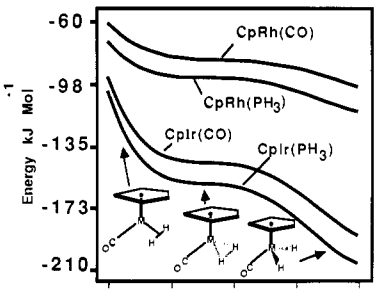

Figure 4. Energy profile for the addition of H_2 to CpRhL and CpIrL with L = CO, PH_3. Left side represents formation of the $Cp(L)MH_2$ adduct with an undistorted H–H bond. Right side represents the formation of a dihydride complex, $Cp(L)M(H)_2$. The plateau at the midpoint of the reaction corresponds to the formation of a dihydrogen complex with an elongated H–H bond.

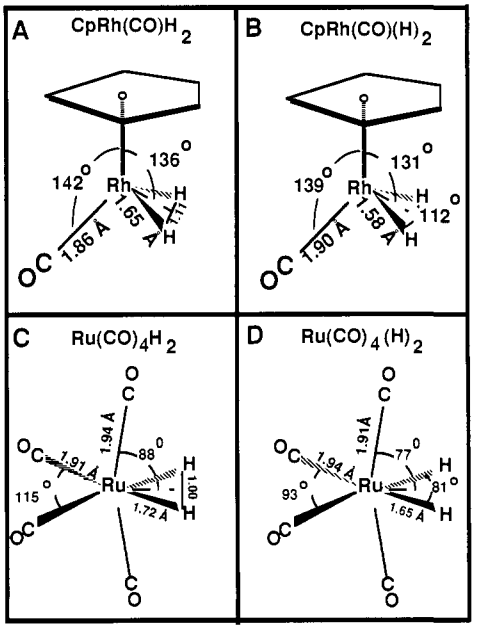

Figure 5. Optimized molecular structures of: (a) the dihydrogen complex $Cp(CO)Rh(H_2)$; (b) the dihydride $Cp(CO)Rh(H)_2$; (c) the dihydrogen complex $Ru(CO)_4(H_2)$; (d) the dihydride $Ru(CO)_4(H)_2$. The homologue 5d systems of iridium and osmium exhibit the same angular features. The homologue 5d systems have similar bond distances (±0.05 Å).

We have studied the reaction in eq 5a by tracing its energy profile, Figure 4. The profiles in Figure 4 represent linear transits in which the internal coordinates are changed linearly from those of the H_2 adduct Cp(L)M-H_2 with fixed H–H distances identical with R(H–H) of free H_2 (left side of Figure 4) to those of the dihydrides, $Cp(L)M(H)_2$ (right side of Figure 4). Eight points were considered in the linear transit. The profiles presented later in Figure 6 for the $M(CO)_4H_2$ systems, with M = Ru, Os, were determined in a similar way. The optimized structure of the dihydride $Cp(CO)Rh(H)_2$ is given in Figure 5.

It follows from Figure 4 that the energy required for the expulsion of H_2 is 100–110 kJ mol^{-1} for M = Rh and 190–210 kJ mol^{-1} for M = Ir. Thus, it should be possible to generate Cp(L)Rh from $Cp(L)Rh(H)_2$ thermally at modest temperatures, whereas the thermal generation of Cp(L)Ir would require rather forcing conditions.

The reaction profiles in Figure 4 exhibit two interesting features. In the first place, we did not find any activation barrier for the addition of H_2 to Cp(L)M. Instead, the still undistorted H_2 molecule is seen to form a rather stable adduct with the Cp(L)M fragment during the early stages of the reaction. The driving force behind the adduct formation, with a formation energy of 60–100 kJ mol^{-1}, is the favorable interaction (**7a**) between the occupied σ_{H_2} orbital of H_2 and the empty 3a' orbital (**2e**) of Cp(L)M. The other interesting feature is the plateau on the energy profile

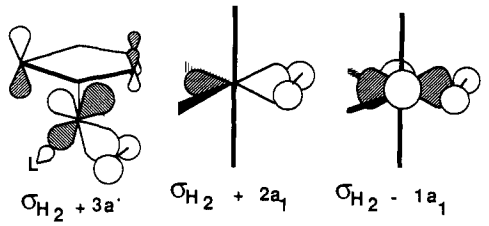

7a **7b** **7c**

midway through the reaction. The plateau represents the formation of a dihydrogen complex. Geometry optimizations revealed that the dihydrogen complexes had a considerably elongated H–H bond with R(H–H) = 1.04–1.12 Å. The optimized structure of $Cp(CO)RhH_2$ is shown in Figure 5a.

The profiles for the reaction

$$M(CO)_4(H)_2 \rightarrow M(CO)_4 + H_2 \qquad M = Ru, Os \quad (5b)$$

are given in Figure 6. The adduct formed early on in the reaction between $M(CO)_4$ and undistorted H_2 is seen to have a rather modest formation energy of less than 3 kJ mol^{-1} (left side of Figure 6). Further, the addition of H_2 to $M(CO)_4$ has a noticeable, albeit small, energy barrier of 3–11 kJ mol^{-1}. Thus, the oxidative addition of H_2 to $M(CO)_4$ (M = Ru, Os) is in the early stages less favorable than the addition of H_2 to Cp(L)M.

The significant differences between the reaction profiles in Figures 4 and 6 can readily be accounted for. In the adduct $M(CO)_4H_2$ there are two interactions between the occupied σ_{H_2} orbital and the metal center. The first, **7b**, is stabilizing and involves the empty 2a$_1$ orbital, **5e**. It parallels closely the interaction **7a** in $Cp(L)MH_2$. The second interaction, **7c**, is two-orbital four-electron repulsive and involves the occupied 1a$_1$ orbital **5c** on $M(CO)_4$. This interaction is largely responsible for the activation barrier and the modest adduct formation energy in the early stages of the addition reaction. The Cp(L)M fragment does not have an occupied d-based orbital with the same nodal σ symmetry as 2a$_1$ (**5e**) of $M(CO)_4$. Consequently, the M–H_2 linkage in $Cp(L)MH_2$ does not suffer a destabilization of the type encountered in **7c**. Yet another factor adding to the difference is the fact that the HOMO 2a″ (**2d**) of Cp(L)M is of higher energy than the HOMO 1b$_2$ (**5d**) of $M(CO)_4$; see Figure 1. Both orbitals will interact, **7d** and **7e**, with the incoming σ^* orbital of

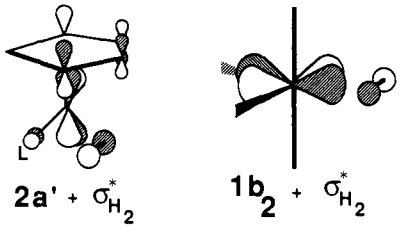

7d **7e**

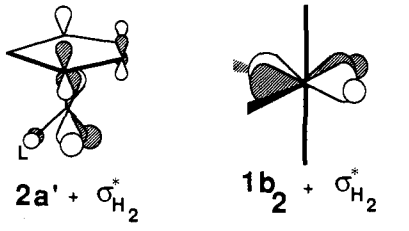

7f **7g**

H_2 under transfer of charge from the metal center to H_2. The higher energy of the HOMO 2a″ (**2d**) of Cp(L)M will, however, make the interaction **7d** more efficient in the early stages of the reaction, since the energy gap between 2a″ and σ^* is smaller. The profiles in Figure 4 do, as a consequence, not exhibit a barrier. Further, the dihydrides $Cp(L)M(H)_2$ have a higher formation energy than the $M(CO)_4(H)_2$ dihydrides since the transfer of charge from 2a″ (**2d**) of Cp(L)M, with the higher energy, to the M–H bonding orbital **7f** is more favorable than transfer of charge from the lower lying 1b$_2$ orbital (**5d**) of $M(CO)_4$ to the M–H bonding orbital **7g**. In simple words, Cp(L)M is more readily oxidized than $M(CO)_4$. A similar argument for the stability of a product from an oxidative addition reaction has been provided by Saillard[5] and Hoffmann. Both reaction profiles in Figure 6 exhibit a plateau, representing the formation of a dihydrogen complex $M(CO)_4H_2$. The dihydrogen complexes have a considerably elongated H–H bond, R(M–H) ~ 1.0 Å as illustrated for $Ru(CO)_4H_2$ in Figure 5c.

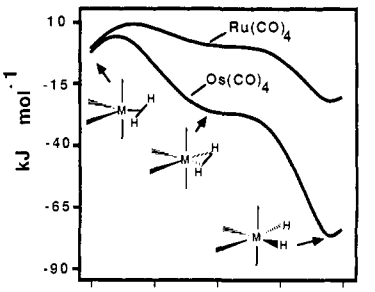

Figure 6. Energy profiles for the addition of H_2 to $Ru(CO)_4$ and $Os(CO)_4$. Left side represents the formation of the $M(CO)_4H_2$ adduct with an undistorted H–H bond. Right side represents the formation of a dihydride complex, $M(CO)_4(H)_2$. The plateau at the midpoint of the reaction corresponds to the formation of a dihydrogen complex with an elongated H–H bond.

Table II. Calculated L_nM–H and L_nM–CH_3 Bond Energies (kJ mol^{-1})

L_nM	$\bar{D}_e$(M–H)[a]	D_e(M–CH_3)[b]
Cp(CO)Rh	285	227
$Cp(PH_3)Rh$	293	229
Cp(CO)Ir	330	260
$Cp(PH_3)Ir$	339	263
$Ru(CO)_4$	246	175
$Os(CO)_4$	274	182

[a] Averaged M–H bond energies in $Cp(L)M(H)_2$. [b] The M–CH_3 bond energies in $Cp(L)M(H)(CH_3)$ and $M(CO)_4(H)(CH_3)$, D_e(M–CH_3), were calculated from $\bar{D}_e$(M–H), the first hydrogen dissociation energy, D_e(CH_3–H), in CH_4, and the reaction enthalpy, ΔH, for the addition of CH_4 to either Cp(L)M or $M(CO)_4$. Thus D_e(M–CH_3) = D_e(CH_3–H) – ΔH – $\bar{D}_e$(M–H).

We find (Figure 6) the dihydride $Ru(CO)(H)_2$ to have a marginal stability of 22 kJ mol^{-1} compared to free H_2 and $Ru(CO)_4$. Experimentally, $Ru(CO)_4(H)_2$ is known[33] to decompose at temperatures above 20 °C. The dihydride $Os(CO)_4(H)_2$ is stable by 76 kJ mol^{-1} (Figure 6), and it does not decompose at room temperature. The enhanced stability of the 5d system is primarily a relativistic effect. The optimized structure of $Ru(CO)_4(H)_2$ is given in Figure 5d. It resembles closely the known structure[34] for $Fe(CO)_4(H)_2$, with the *trans*-carbonyl groups bent toward the hydrogens.

Calculated averaged metal–hydrogen bond energies are compiled in Table II. The calculated order of stability for the M–H bonds in the dihydrides is $\bar{D}_e$(Ir–H) > $\bar{D}_e$(Rh–H) > $\bar{D}_e$(Os–H) > $\bar{D}_e$(Ru–H). The M–H bonds in the $M(CO)_4(H)_2$ systems are relatively weaker due to the destabilizing influence of the 1a$_1$ orbital (**5c**) as well as the higher energy of the 2a orbital (**2d**) of Cp(L)M. Within a homologous series, the 5d metal forms the stronger M–H bond as a result of relativistic effects and better bonding overlaps. Stoutland[1] et al. have estimated the averaged Ir–H bond energy in $(\eta^5\text{-}Me_5C_5)(PMe_3)Ir(H)_2$ to be 310 kJ mol^{-1} in fair agreement with our calculated value of $\bar{D}_e$(Ir–H) = 339 kJ mol^{-1} for $Cp(PH_3)Ir(H)_2$. Calderazzo[35] has provided a rough estimate of the averaged Os–H bond energy in $Os(CO)_4(H)_2$ of

(33) Cotton, J. D.; Bruce, M. I.; Stone, F. G. A. *J. Chem. Soc. A* **1968**, 2162.
(34) McNeil, E. A.; Scholer, F. R. *J. Am. Chem. Soc.* **1977**, *99*, 6243.
(35) Calderazzo, R. *Ann. N.Y. Acad. Sci.* **1983**, *415*, 37.

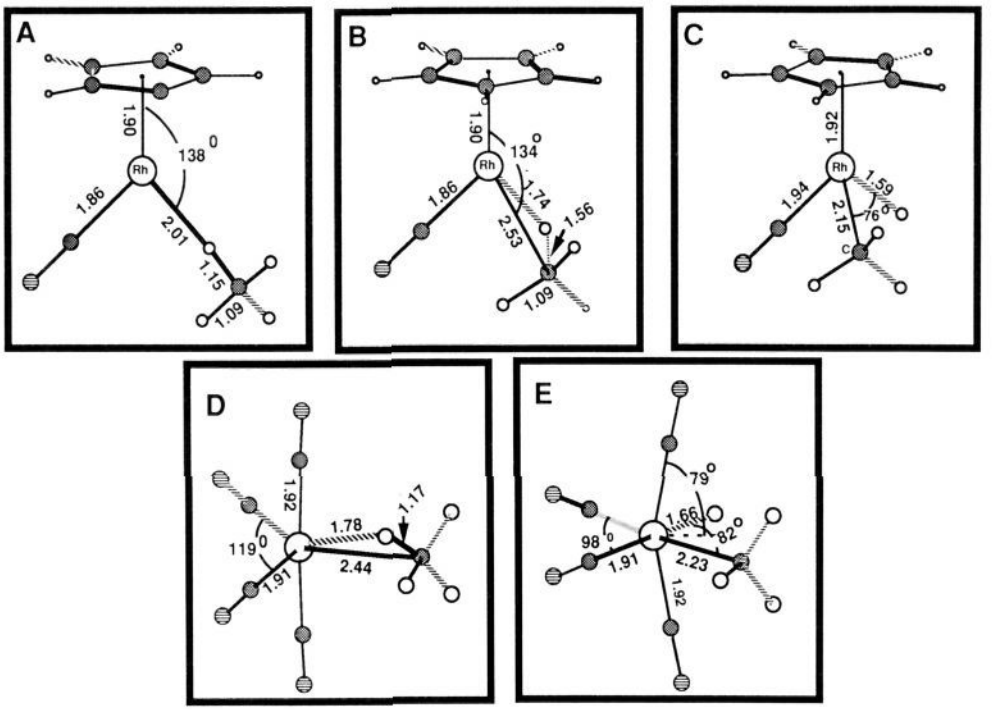

Figure 7. Optimized molecular structures of: (a) adduct between CH_4 and CpRh(CO); (b) transition state for the oxidative addition of CH_4 to CpRh(CO); (c) Cp(CO)Rh(H)(CH_3); (d) transition state for the oxidative addition of CH_4 to $Ru(CO)_4$; (e) $(CO)_4Ru(H)(CH_3)$. The homologue 5d systems of iridium and osmium exhibit the same angular features. The homologue 5d systems have similar bond distances (±0.05 Å). Bond distances are in angstroms.

326 kJ mol^{-1}, which is somewhat higher than our calculated value of 274 kJ mol^{-1}. We feel, on the basis of the analysis given above, that the Ir–H bond should be stronger than the Os–H bond.

V. Activation of the C–H Bond in CH_4 by Cp(L)M and $M(CO)_4$

The addition of a C–H methane bond to $(C_5Me_5)IrL$ has been accomplished by Graham[36] et al. for L = CO and by Bergman[37] et al. for L = PMe_3. It is a remarkably facile process, which can take place even at 12 K, as demonstrated by Rest and Graham.[38] The CpIrL and CpRhL systems are among the few late-transition-metal fragments capable of activating an alkylic C–H bond. Many other late-transition-metal systems do not exhibit the same reactivity toward alkylic C–H bond, although they might add H_2 oxidatively. We shall in the following attempt to unravel the unique features of the Cp(L)M species by tracing the energy profiles for the reaction

$$Cp(L)M + CH_4 \rightarrow Cp(L)M(H)(CH_3) \qquad M = Rh, Ir;\ L = CO, PH_3 \quad (6a)$$

We shall further investigate whether the isolobal[5] $M(CO)_4$ (M = Ru, Os) systems are able to add a C–H bond oxidatively by tracing the energy profiles for the reaction

$$M(CO)_4 + CH_4 \rightarrow M(CO)_4(H)(CH_3) \qquad M = Ru, Os \quad (6b)$$

The incoming CH_4 molecule forms, in the early stages of the reaction in eq 6a, a σ adduct with the Cp(L)M fragment. The optimized structure of this adduct is given in Figure 7a for Cp(CO)Rh(H–CH_3). We note a modest elongation of the C–H bond coordinated end-on to the metal center. Adduct formation energies for Cp(L)M(H–CH_3) are displayed in Table III. They range from 59–51 kJ mol^{-1} for M = Ir to 29–24 kJ mol^{-1} for M = Rh. The driving force behind the adduct formation is clearly the favorable interaction, **8a**, between the occupied σ_{CH_4} orbital on CH_4 and the empty 3a′ orbital, **2e**, on Cp(L)M. The involvement of a σ adduct as an intermediate in the reaction of eq 6a has already been predicted by Bergman et al.[39]

Table III. Calculated Reaction Enthalpies, ΔH, and Adduct Formation Energies, ΔE_{add}, for the Addition of CH_4 to CpML and $M(CO)_4$

L_nM	ΔH, kJ mol^{-1}	ΔE_{add}, kJ mol^{-1}
Cp(CO)Rh	−62[a]	29[b]
$Cp(PH_3)Rh$	−72	24
Cp(CO)Ir	−140	59
$Cp(Ph_3)Ir$	−152	51
$Ru(CO)_4$	29	1
$Os(CO)_4$	−6	2

[a] Stability of the σ-adduct $L_nM(H–CH_3)$ compared to CH_4 and ML_n. [b] Reaction enthalpy for the addition of CH_4 to L_nM.

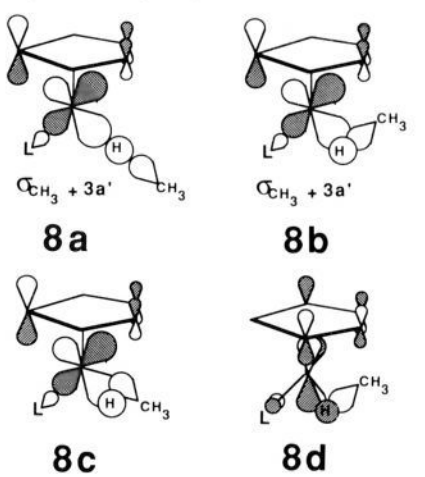

(36) Hoyano, J. K.; McMaster, A. D.; Graham, W. A. *J. Am. Chem. Soc.* **1983**, *105*, 7190.
(37) Wax, M. J.; Stryker, J. M.; Buchanan, J. M.; Kovac, C. A.; Bergman, R. G. *J. Am. Chem. Soc.* **1984**, *106*, 1121.
(38) Rest, A. J.; Whitwell, I.; Graham, W. A. G.; Hoyano, J. K.; McMaster, A. D. *J. Chem. Soc., Chem. Commun.* **1984**, 624.
(39) Buchanan, J. M.; Stryker, J. M.; Bergman, R. G. *J. Am. Chem. Soc.* **1986**, *108*, 1537.

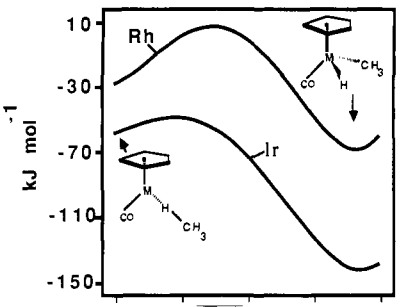

Figure 8. Energy profile for the addition of CH_4 to CpRhCO and CpIrCO. Left side gives energy of adduct between CH_4 and CpMCO. Right side gives the energy of $Cp(CO)M(H)(CH_3)$. All energies are relative to CH_4 and CpM(CO) at infinite separation.

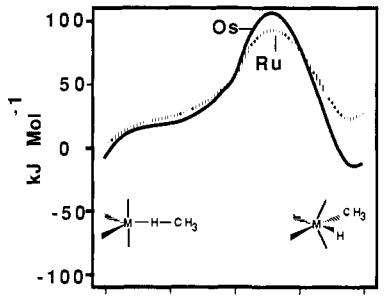

Figure 9. Energy profiles for the addition of CH_4 to $Ru(CO)_4$ and $Os(CO)_4$. Left side gives energy of adduct between CH_4 and $M(CO)_4$. Right side gives energy of $(CO)_4M(H)(CH_3)$. All energies are relative to CH_4 and $M(CO)_4$ at infinite separation.

The energy profile for the remainder of the process is traced in Figure 8 for L = CO and M = Ir, Rh. The profiles were obtained by gradually moving the hydrogen atom, in the C–H bond attached end-on to the metal center, from the position it had in the σ adduct, Figure 7a, to its position in the resulting hydrido–alkyl complex, Figure 7c. For each move of the hydrogen atom all degrees of freedom were optimized except for the internal Cp coordinates. A total of eight moves of the hydrogen atom were considered. The profiles shown in Figure 9 for the $M(CO)_4(H)(CH_3)$ systems, with M = Ru, Os, were determined in a similar way. Total reaction enthalpies for each of the processes in eq 6a are displayed in Table III.

It follows from Figure 8 and Table III that the reaction for M = Ir has a modest activation barrier of 10 kJ mol^{-1} with a reaction enthalpy of −140 to −150 kJ mol^{-1}. The activation barrier for the rhodium systems is somewhat higher at 37 kJ mol^{-1} and the reaction enthalpy less favorable at between −70 and −60 kJ mol^{-1}. Our findings here are in agreement with the general experimental observation that the 5d species Cp(L)Ir activates alkylic C–H bonds more readily than the 4d homologues, Cp(L)Rh. The differential is caused by relativistic effects as well as the 5d elements' ability to form stronger σ overlaps with $1s_H$ and σ_{CH_3}, **8c**. Stoutland[1] et al. have carried out a detailed experimental analysis of the energetics involved in the C–H activation by $(C_5Me_5)Ir(PMe_3)$. They infer a small barrier of 8–40 kJ mol^{-1} and a reaction enthalpy of −110 to −120 kJ mol^{-1}, in fair agreement with our findings. Jones[4a] and Feher have investigated the energetics for the addition of CH_4 to the corresponding rhodium system, $(C_5Me_5)Rh(PMe_3)$. Their data are consistent with a reaction enthalpy[40] of −40 to −30 kJ mol^{-1} and an upper limit[41] of 20 kJ mol^{-1} for the activation energy.

What makes the Cp(L)M systems unique is the uninhibited stabilizing intervention of the 3a′ orbital (**2e**) throughout the reaction in eq 6a. That is, the empty 3a′ orbital will stabilize the electron pair, originally in the C–H bond approaching the metal center, from the formation of the σ adduct (**8a**), over the transition state (**8b**), to the final hydrido–methyl complex, Figure 7c, where the pair resides in an orbital (**8c**) made up of in-phase combinations between 3a′ (**2e**) and $1s_H$ as well as σ_{CH_3}. The other favorable factor is the high energy of the 2a″ orbital (**2d**) on Cp(L)M, Figure 1, which makes it possible for 2a″ to interact (**8d**) stabilizing with the incoming σ^* orbital of CH_4 early on in the reaction. The approximate transition-state structure for the process involving Cp(CO)Rh is shown in Figure 7b. It has the characteristic three-center pattern postulated by several investigators, with a considerably elongated C–H bond of R(C–H) = 1.56 Å. The elongation is primarely due to the interaction **8d**. We should also note that the product from the oxidative addition in eq 6c is rather stable compared to the reactants due to the relatively high energy of the 2a″ orbital (**2d**) on Cp(L)M, as explained in section IV.

The energy profiles for the processes in eq 6b, between CH_4 and $M(CO)_4$ (M = Ru, Os), are given in Figure 9. There is early on in the reaction an almost negligible stabilization of 1–2 kJ mol^{-1}, Table III, due to the formation of a σ adduct between CH_4 and $M(CO)_4$. The energy rises steeply as the process progresses further to an activation barrier of 101 kJ mol^{-1} for M = Os and 79 kJ mol^{-1} for M = Ru. The total reaction enthalpy is 28 kJ mol^{-1} for the ruthenium system and −6 kJ mol^{-1} for the osmium system. Thus $(CO)_4Ru(H)(CH_3)$ is seen to be unstable with respect to CH_4 and $Ru(CO)_4$ and is unlikely to be produced from the process in eq 6b. It might be synthesized by other means. However, $(CO)_4Ru(H)(CH_3)$ seems not to have been isolated. It is also unlikely that the osmium system should be produced from the reaction in eq 6b. It has been synthesized by an alternative route. It is relatively unstable and eliminates CH_4 on heating.[42]

The reaction in eq 6b is stabilized throughout the oxidative addition by the empty $2a_1$ orbital **5e** in a manner that resembles the interventions (**8a–c**) of 3a′ (**2e**) in the addition reaction of eq 6a. However, the former reaction is inhibited by the occupied $1a_1$ orbital **2c**. This orbital will interact in a four-electron two-orbital destabilizing fashion with the incoming σ_{CH_4} orbital in the σ adduct (**9a**) as well as the transition state, **9b**. The $1a_1$ orbital

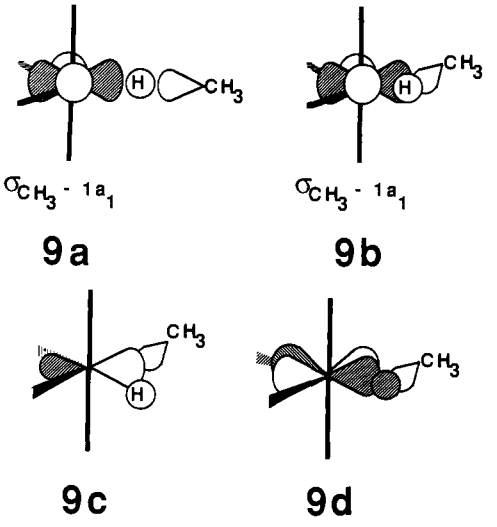

will also destabilize the electron pair residing in the orbital **9c** of the final hydrido–alkyl product $(CO)_4M(H)(CH_3)$ by yet another four-electron two-orbital repulsive interaction. That is, **9c** must be orthogonal to $1a_1$ (**2c**) and thus mix in $1a_1$ in an out-of-phase manner. The Cp(L)M fragment does not have a counterpart to $1a_1$, and the Cp(L)M species is for this reason a more powerful agent for the activation of alkylic C–H bonds. Also, the $1b_2$ orbital (**5d**) of $M(CO)_4$ has a relatively low energy, Figure 1. The interaction (**9d**) between $1b_2$ and the incoming σ^* orbital on CH_4 is as a consequence not very strong in the early stages of the addition reaction. The absence of any strong interaction in **9d**

(40) Deduced from Figure 6 of ref 4a under the assumption that ΔS for the reaction is −30 eu as suggested in ref 4a.

(41) A free energy of activation of 20 kJ mol^{-1} can be deduced from Figure 6 of ref 4a. This is an upper bound to the activation energy, granted that the entropy of activation is negative.

(42) Norton, J. R. *Acc. Chem. Res.* **1979**, *12*, 139.

will further add to the activation barrier. The transition-state structure for the addition of CH_4 to $Ru(CO)_4$ is given in Figure 7e. Note the modest elongation of the C-H bond, $R(H-CH_3)$ = 1.17 Å, as a result of the weak interaction in **9d**. The low energy of the $1b_2$ orbital (**5d**) on $M(CO)_4$ is also contributing to the fact that $M(CO)_4(H)(CH_3)$ is less stable than $Cp(L)(H)(CH_3)$.

The calculated $M-CH_3$ bond energies are given in Table II. The strength of the $M-CH_3$ bonds follows the order $D(Ir-CH_3) > D(Rh-CH_3) > D(Os-CH_3) > D(Ru-CH_3)$. This order is determined by the same factors as the analogous order for the corresponding M-H bonds; see section IV and Table II. The $M-CH_3$ linkages are consistently weaker than the corresponding M-H bonds by 60-100 kJ mol^{-1}. This differential, which is characteristic for late-transition metals, has been rationalized in a previous study.[12] The calculated $Ir-CH_3$ bond strength of 260 kJ in $Cp(PH_3)Ir(H)(CH_3)$ is in line with the experimental value of 235 kJ mol^{-1} obtained by Stoutland[1] et al. in $(C_5Me_5)(PMe_3)Ir(CH_3)_2$. It is exceptionally high, attesting to the unique features of the Cp(L)Ir system discussed above. Other $Ir-CH_3$ bonds are much weaker. Thus, $D(Ir-CH_3)$ in $(PMe_3)_2(CO)Ir(I)(Cl)(CH_3$ is measured[1] to be 148 kJ mol^{-1}, which is comparable to our calculated $D(Os-CH_3)$ value of 182 kJ mol^{-1} in the isoelectronic $Os(CO)_4(H)(CH_3)$ system. In both systems the $M-CH_3$ linkage is destabilized by the interaction of a fully occupied d-based orbital, **2c**.

VI. Concluding Remarks

We have, in the present study, investigated the molecular and electronic structures of the coordinatively unsaturated d^8 fragments Cp(L)M and $M(CO)_4$, as well as their potentials as catalysts in the functionalization of CH_4 according to Scheme I. We have found that the Cp(L)M fragments are unique as C-H activating agents, step b of Scheme I, in that they only have empty d-based orbitals interacting with the incoming C-H bond. Most other mononuclear d^8 systems, including the $M(CO)_4$ systems, have empty as well as occupied metal-based orbitals, and the latter will impede the addition reaction in step b. Further, the fact that the 2a″ HOMO (**2e**) has a relatively high energy helps reduce the energy barrier for the addition of H-H and $H-CH_3$ bonds. The high energy of 2a″ is further instrumental in stabilizing the products from the oxidative addition reactions. The generation of the active species Cp(L)M, step a of Scheme I, from the coordinatively saturated Cp(L)MZ system was investigated in some detail for Z = CO, PH_3, and H_2. It was concluded that too much energy, in the order of 200 kJ mol^{-1}, is required for step a with Z = CO. The step is more favorable for $Z = H_2$ and in particular $Z = PH_3$. We have assumed that the C-H bond in CH_4 is activated by a 16-electron species. Marx[43] and Lees have recently suggested that $CpIr(CO)_2$ might activate CH_4 by an associative mechanism without prior loss of CO. The mechanism suggested by Marx and Lees has not been investigated in the present study.

Acknowledgment. This investigation was supported by the Natural Sciences and Engineering Research Council of Canada (NSERC). We thank Professor E. J. Baerends and Professor W. Ravenek for a copy of their vectorized LCAO-HFS program system and the University of Calgary for access to their Cyber-205 facility.

Registry No. $Cp(CO)Rh(H)_2$, 122699-95-0; $Cp(PH_3)Rh(H)_2$, 122699-96-1; $Cp(CO)Ir(H)_2$, 78829-47-7; $Cp(PH_3)Ir(H)_2$, 87966-29-8; *cis*-$Ru(CO)_4(H)_2$, 21029-23-2; *cis*-$Os(CO)_4(H)_2$, 18972-42-4; $Cp(CO)Rh(H)(CH_3)$, 108582-17-8; $Cp(PH_3)Rh(H)(CH_3)$, 122699-97-2; $Cp(CO)Ir(H)(CH_3)$, 87739-22-8; $Cp(PH_3)Ir(H)(CH_3)$, 122699-98-3; *cis*-$Ru(CO)_4(H)(CH_3)$, 122699-99-4; *cis*-$Os(CO)_4(H)(CH_3)$, 22639-03-8; Cp(CO)Rh, 86803-04-5; $Cp(PH_3)Rh$, 86803-01-2; Cp(CO)Ir, 87966-32-3; $Cp(PH_3)Ir$, 87966-30-1; $Ru(CO)_4$, 29718-13-6; $Os(CO)_4$, 27857-69-8; $Cp(CO)_2Rh$, 12192-97-1; $Cp(PH_3)(CO)Rh$, 122700-00-9; $Cp(CO)_2Ir$, 12192-96-0; $Cp(PH_3)_2Rh$, 122700-01-0; $Cp(PH_3)(CO)Ir$, 122700-02-1; $Cp(PH_3)_2Ir$, 122700-03-2.

(43) Marx, D. E.; Lees, A. L. *Inorg. Chem.* **1988**, *27*, 1121.

Electrochemistry of Cytochrome *c*, Plastocyanin, and Ferredoxin at Edge- and Basal-Plane Graphite Electrodes Interpreted via a Model Based on Electron Transfer at Electroactive Sites of Microscopic Dimensions in Size

Fraser A. Armstrong, Alan M. Bond,[1] H. Allen O. Hill,* B. Nigel Oliver, and Ioanna S. M. Psalti

Contribution from the Inorganic Chemistry Laboratory and the Oxford Centre for Molecular Sciences, South Parks Road, Oxford, OX1 3QR, Great Britain. *Received November 30, 1988*

Abstract: The electrochemistry of a range of electron-transfer proteins at edge- and basal-plane graphite electrodes has been reconsidered using a *microscopic* model, which involves fast electron transfer at very small oxygen-containing electroactive surface sites. This model assumes that mass transport to the electrode occurs by radial diffusion when the density of the surface active sites is low (as is generally true in the case of the basal-plane graphite electrode) and by linear diffusion when the density of the active sites is increased sufficiently to cause overlap of the diffusion layers. With this model it is now proposed that the electrochemistry of cytochrome *c*, plastocyanin, and ferredoxin occurs with a very fast rate of charge transfer ($\geq$1 cm s^{-1}) at both edge- and basal-plane graphite electrodes. Critical factors, such as the mode of surface preparation (including covalent derivatization), the pH, and the presence in the electrolyte of cations such as Mg^{2+} or $Cr(NH_3)_6^{3+}$, control the *density* of surface sites, which result in the electrochemistry of a specific protein. This contrasts with the conclusion that has been reached previously based upon a conventional macroscopic model, which supposes that the *rate* of electron transfer is subject to enhancement or depression through these factors. The proposal that the electron-transfer process at the protein–graphite electrode interface is very fast over a wide range of conditions is now consistent with homogeneous kinetic studies where electron-transfer reactions of proteins, particularly amongst physiological partners, are also known to be fast.

Chemical and electrochemical studies of redox proteins have attracted considerable attention over the last few years.[2-5] Generally, homogeneous rates of electron transfer have been found to be fast. In contrast, heterogeneous rates of electron transfer

0002-7863/89/1511-9185$01.50/0